NRIAG Journal of Astronomy and Geophysics 7 (2018) 334–346

Contents lists available at ScienceDirect

NRIAG Journal of Astronomy and Geophysics

journal homepage: www.elsevier.com/locate/nrjag

Full length article

# Structural study using 2D modeling of the potential field data and GIS technique in Sohag Governorate and its surroundings, Upper Egypt

Hosni H. Ghazala[a], Ismael M. Ibraheem[b,*], M Lamees[a], Menna Haggag[a]

[a] Department of Geology, Fac. of Science, Mansoura University, Mansoura 35116, Egypt
[b] Institute of Geophysics and Meteorology, University of Cologne, Pohligstr. 3, 50969 Cologne, Germany

ARTICLE INFO

*Keywords:*
Sohag
GIS
Gravity
Magnetic
2D forward modeling
Tilt derivative

ABSTRACT

The main purpose of the present study is to identify the surface and subsurface structural features and configuration of the basement in the area around Sohag Governorate using Geographic Information System (GIS) and potential field data (gravity and aeromagnetic). The hill shade was found as the most suitable image for surface lineament delineation and to produce a fault potential prediction map using the overlay model technique. The subsurface faults and contacts were detected and traced out from the reduced to the pole (RTP) magnetic, Bouguer gravity anomaly, and tilt derivative maps. The basement structural map of study area has been created based on tilt derivative technique. The structural tectonic maps show that the E-W, NNW-SSE, and NNE-SSW directions are the main trends affecting the study area. The subsurface configuration of the basement was detected using two dimensional (2D) gravity and magnetic forward modeling along preselected six long profiles crossing the study area. The 2D models suggest a depth range to the basement of 400 to 4000 m.

## 1. Introduction

The Egyptian Government has initiated a long-term development strategy for the development of Upper Egypt and has recently witnessed an upsurge in concern for the environment and its natural components. Therefore, the scientists and researchers should involve in the research activities in this sector to get the maximum benefit from development projects. From this point, The interpretation of potential field data (gravity and magnetic) and GIS techniques were used to shed more light on the surface and subsurface features as well as the thickness of the sedimentary cover in the area of Sohag Governorate and its surroundings.

The investigated area located along El-Hmaima-Balyana sector extends between longitudes 31°00′ to 32°00′E and latitudes 26°00′ to 27°00′N including both the floodplain and the desert fringes (Fig. 1). The main aim of this study is to delineate the surface and subsurface structures of Sohag Governorate and to estimate the depths to the basement surface using potential field and GIS techniques.

## 2. Geological and structural setting

According to Ganoub El-Wadi Petroleum Holding Company's report of Balyana-1 well, the area of study is characterized by a thick sedimentary section ranging in age from Late Cretaceous represented by the Nubia sandstone (Coniacian-Campanian) to Quaternary (Yehia et al., 1999). It unconformably overlies the Precambrian basement rocks that crop out in high mountains of Eastern Desert. The basement rocks mainly consist of metamorphic and metavolcanic rocks, intruded by pink or gray granites which dissected by dikes (Said, 1962; Said et al., 1970; Wendorf and Schild, 1976). The alkali olivine basalts of Tertiary volcanics are exposed in the southeast Qena sector (Yehia et al., 1999).

The surface geology (Fig. 2) was extracted from the geologic map of Egypt (Conoco, 1987). The sedimentary succession is represented by Tarawan and Esna Formations, which belong to the Paleocene and Early Eocene, respectively. Tarawan Formation is composed of white chalky limestone, containing beds of marl. Esna Formation consists of greenish-gray shale with calcareous towards the top, overlaying the Thebes group of the Lower Eocene.

The Thebes group is consisting of three formations: Sarai, El-Rufuf and Dunka. Sarai Formation is thin chalky limestone rich in chert bands and concretions. El-Rufuf Formation consists of limestone with an increasing content of brown chert bands. At the top, is Drunka Formation that consists of dense, thickly limestone, locally reefal and local flint bands.

The Pliocene Epoch is represented by Issawia Formation which

Peer review under responsibility of National Research Institute of Astronomy and Geophysics.
* Corresponding author at: Institute of Geophysics and Meteorology - University of Cologne Pohligstrsse 3 (Office 3.235), 50969 Cologne, Germany.
*E-mail address:* ismael.ibraheem@geo.uni-koeln.de (I.M. Ibraheem).

https://doi.org/10.1016/j.nrjag.2018.05.008
Received 1 March 2018; Received in revised form 19 May 2018; Accepted 24 May 2018
Available online 07 June 2018

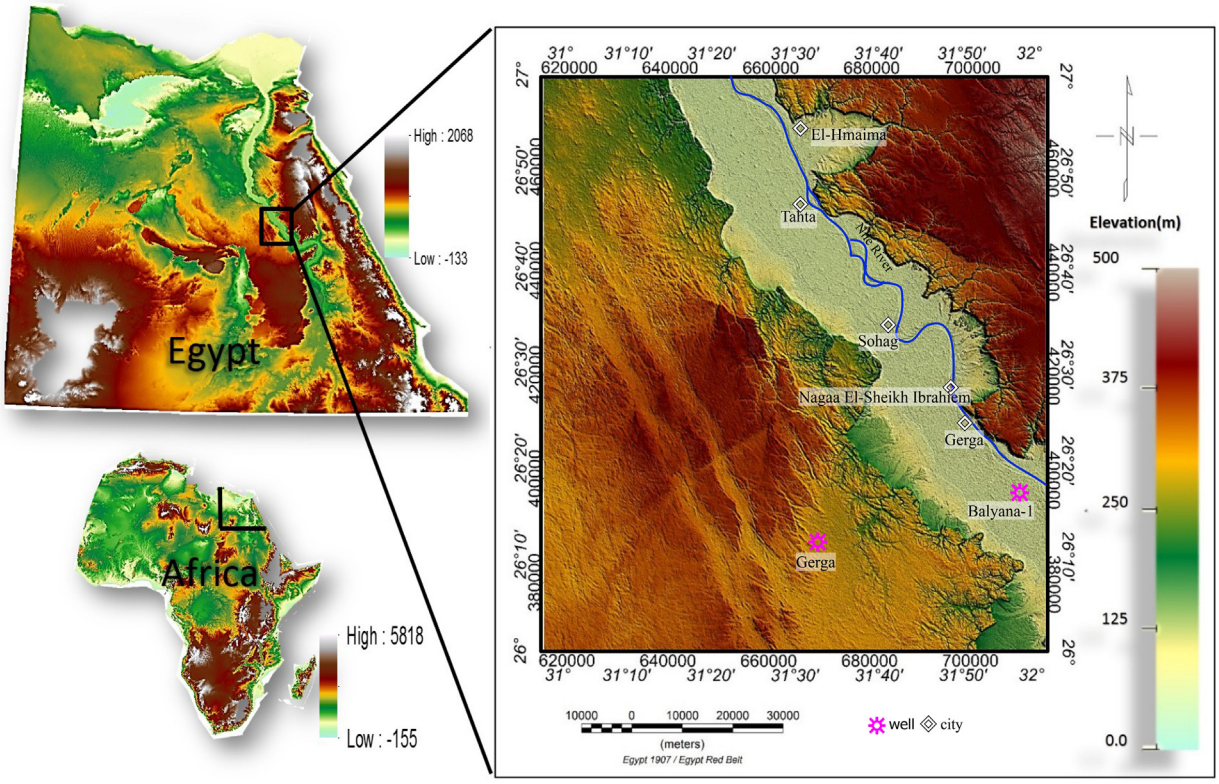


**Fig. 1.** ASTER digital elevation model (DEM) of the study area.

consists of siltstone with clay-stone, limestone and sandstone. Said (1962) mentioned that the Quaternary and Recent deposits are represented by Pre-Nile deposits, Wadi deposits and Playa deposits. Pre-Nile deposits are composed of sediments which contain the horizontal Pleistocene Reefal limestone.

Structurally, The surveyed area lies within the stable shelf of Egypt. The fault trends affecting the stable shelf area are categorized into four sets: E-W, NE- SW, N-S, and NW-SE (Said, 1962). The Nile river is occupied by graben that created by up-throw of the eastern and western plateaus. NW-SE fractures has been interpreted as conjugated sets due to the compression stress originated in the NNE direction (Youssef, 1968).

## 3. Surface structures using GIS technique

GIS is an essential application tool with potentially far- reaching application in the field of geological science because of the fundamental properties of geological features; the two horizontal dimensions (x, y coordinates), the third dimension (z height), and the fourth dimension (time) (El-Sherief, 2016).

In the present study, the GIS technique has been used to delineate the structural features, such as faults and contacts. This field is determined as an arid area which made it laborious to pull out and detect its structural characteristics. There is a direct link between the presence of faults in any area and the displacement of rock layers. Moreover, the existence of faults may be represented by some geological features such as drainage patterns, lineaments (linear features), and lithological contacts between rock units (Abdullah et al., 2013).

Four contributing factors; drainage patterns, faults (previously mapped), lineaments, and lithological contacts were the main parameters used in this study. Different image processing techniques were applied to delineate fault segments using Advanced Space Borne Thermal Emission and Reflection Radiometer (ASTER) and Global Digital Elevation Model (GDEM) (spatial resolution: 30 m), with raster format. ASTER and GDEM were provided in geographic projection referenced to the UTM datum and WGS84 system. The data extracted from these images together with the topographic maps, the geological maps, and the available information extracted from previous literatures were introduced in the GIS environment.

The most important feature in the study area is the presence of drainage lines patterns and fault lines. A strong relationship between these fault lines and drainage pattern system distribution is clear in the area (Abdullah et al., 2013).

The DEMs data were used for automatic extraction of drainage patterns over the study area. The stream network is created after the determination of the flow direction and the flow accumulation in every cell, by using a starting value, which is the minimum catchment area in the stream network. The stream network was obtained by connecting the cells in which the flow accumulation is higher than the starting value. With a lower starting value, the density of the network increases (Mao et al., 2014). In the present study, we used stream cell unit of 1000 units. The output data channel will appear as lines representing the rivers and streams (Fig. 3).

The fault map of the study area was extracted from the digital elevation model after converted to fault buffer layer and then converted to slicing layer to produce the shaded relief map (Fig. 4). This layer was

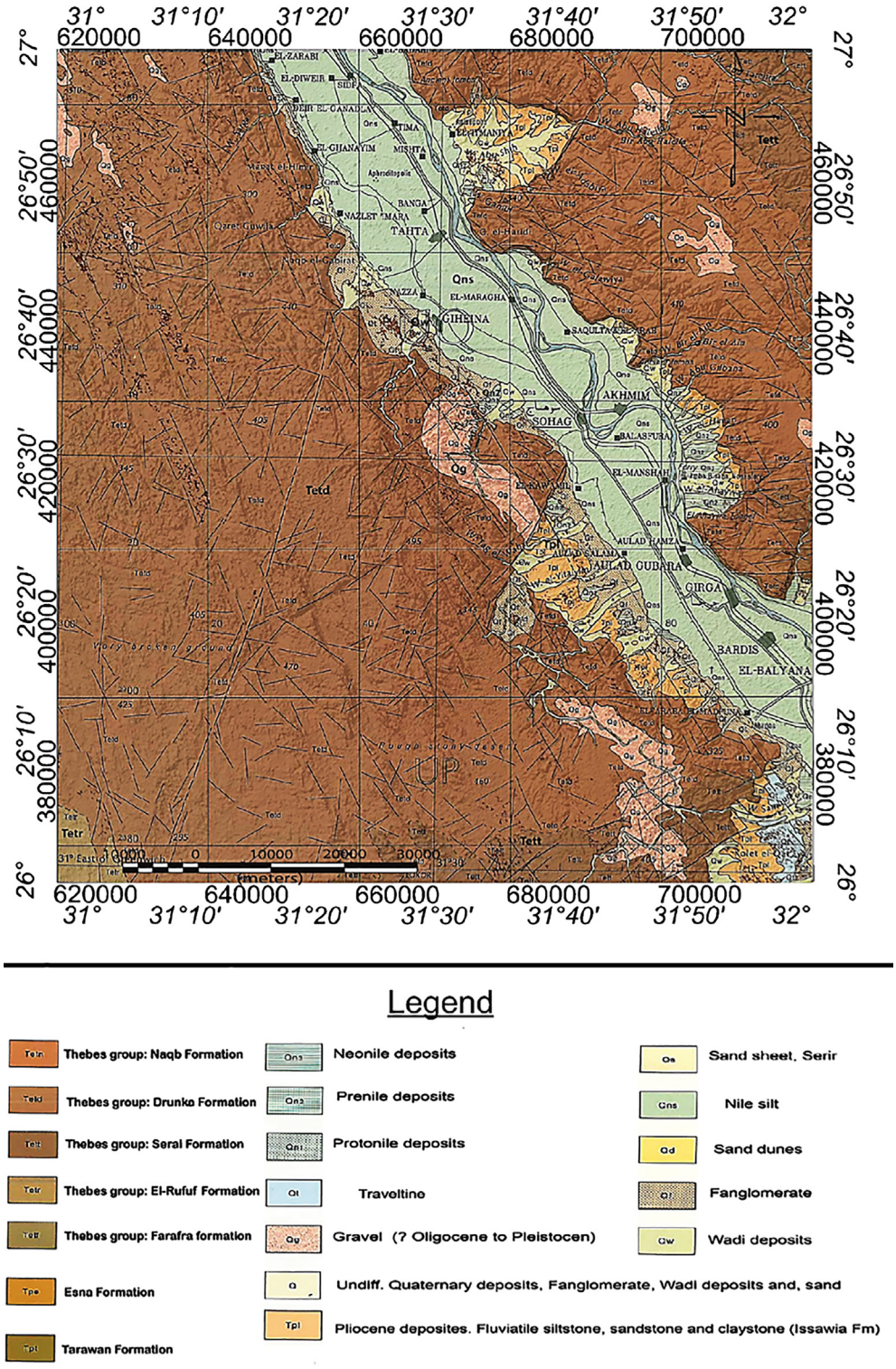


## Legend

- Teln — Thebes group: Naqb Formation
- Teld — Thebes group: Drunka Formation
- Tets — Thebes group: Seral Formation
- Telr — Thebes group: El-Rufuf Formation
- Telf — Thebes group: Farafra formation
- Tpe — Esna Formation
- Tpl — Tarawan Formation
- Qns — Neonile deposits
- Qns — Prenile deposits
- Qnl — Protonile deposits
- Qt — Travertine
- Qg — Gravel (? Oligocene to Pleistocen)
- Q — Undiff. Quaternary deposits, Fanglomerate, Wadi deposits and, sand
- Tpl — Pliocene deposites. Fluviatile siltstone, sandstone and claystone (Issawia Fm)
- Qs — Sand sheet, Serir
- Qns — Nile silt
- Qd — Sand dunes
- Qf — Fanglomerate
- Qw — Wadi deposits

**Fig. 2.** The geological map of the study area (after Conoco, 1987).

added to the GIS model. In the present study, the overlay layers for the model were used in extraction of the structural elements and to detect the lineaments during the interpretation process (Fig. 5a). A rose diagram (Fig. 5b) was drawn to determine the fault trends in the study area where it shows that the surface structural trends are E-W (Mediterranean Sea trend), NNW-SSE, and NNE-SSW (Aqaba trend), in addition to minor trends in ENE-WSW and WNW-ESE directions. E-W direction represents the major trend in the study area. These trends correspond in

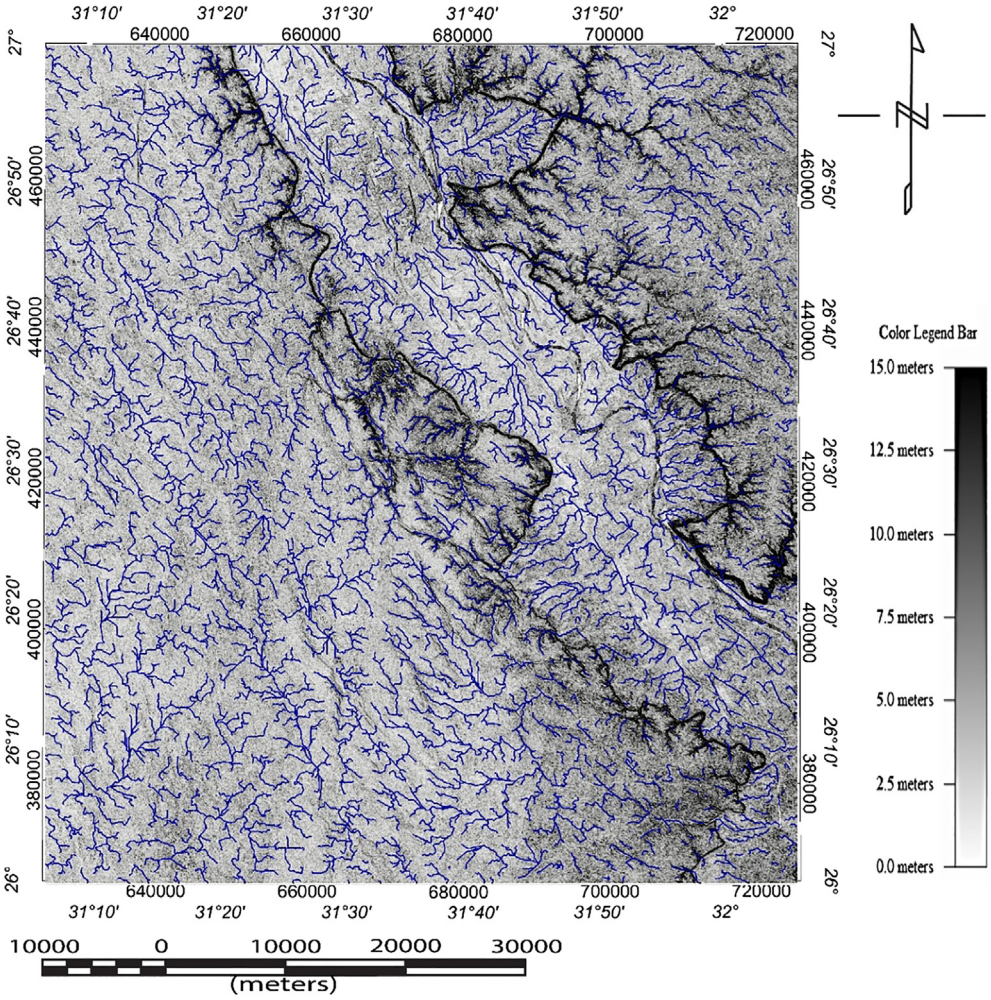


**Fig. 3.** The slope shade map of the ASTER DEM shows the drainage stream network represented by the blue lines with stream cell unit of 1000 units. (For interpretation of the references to colour in this figure legend, the reader is referred to the web version of this article.)

somehow with the trends mentioned by Said (1962).

## 4. Potential field data

The primary goal of using potential field data is to provide a better understanding of the subsurface structure of the study area. Gravity and magnetic methods are relatively cheap, non-invasive, and non-destructive remote sensing method (Telford et al., 1990). Moreover, gravity and magnetic data provide information about densities and magnetic susceptibilities variations of the rocks. Geologists and geophysicists can make inferences about the distribution of strata that may be favorable for trapping oil and gas because of the presence of wide range in densities and magnetic susceptibilities among rock types. Furthermore, because faults commonly juxtapose rocks of differing densities and/or susceptibilities, the gravity and magnetic methods are an excellent exploration choice (Ibraheem, 2009).

The gravity and aeromagnetic surveys were carried out by the General Petroleum Company (1977) and the Aero Service Division of the Western Geophysical Company of America (1983), respectively. The aeromagnetic survey was carried out by flight altitude of 914.4 m barometric with direction of 45°/225°, inclination of 39.5°N, and declination of 2.0°E. The gravity and aeromagnetic data were digitalized and converted to the Bouguer gravity and total magnetic intensity maps.

The Bouguer gravity anomaly map was compiled from four sheets with a scale of 1:100,000 and contour interval of 1 mGal to form a grid composed of 71,899 values (Fig. 6). Moreover, The total magnetic intensity map was compiled from three sheets with a scale of 1:50,000 and contour interval of 10 nT. They were digitized to form a grid composed of 809,350 values (Fig. 7).

The aeromagnetic data was reduced to the north magnetic pole (Fig. 8) to make the dipolar magnetic anomalies transform to monopolar anomalies centered over their causative bodies and the actual inclination is changed to the vertical direction. Accordingly, all of the magnetic anomalies of the RTP map are re-arranged themselves to the north direction to remove the skewness in the magnetic field to make the anomalies overlie directly over their sources (Ibraheem et al., 2018a).

### 4.1. Tilt derivative technique

The tilt derivative (TDR) is the ratio of the first vertical derivative of

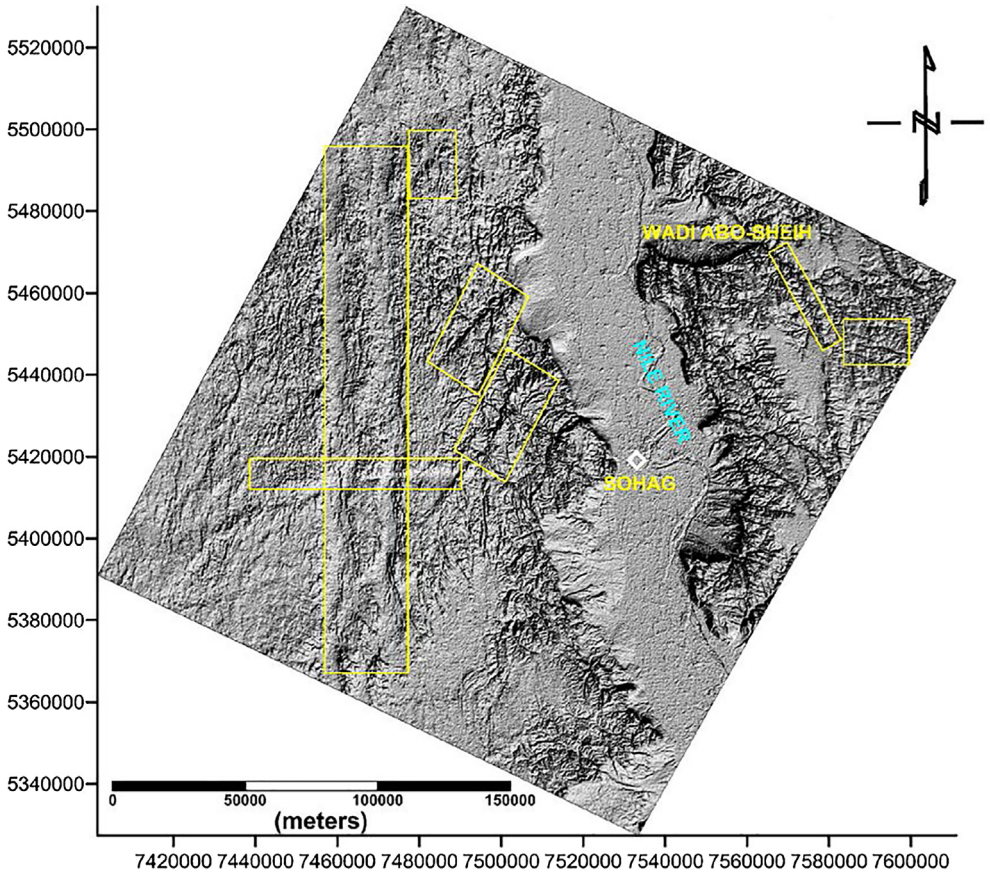


**Fig. 4.** The grey-shaded relief map from the ASTER DEM map of the study area shows the main faults affects the study area.

the potential field and the magnitudes of the horizontal gradient (Oruç and Keskinsezer, 2008). The TDR technique is employed for mapping basement structures and to define the boundary of causative sources (Ibraheem et al., 2018b). It is considered as a powerful method for edge detection (Ibraheem, 2005; Shahverdi et al., 2017). The TDR equation adopted in the TDR technique designation is as follows (Miller and Singh, 1994):

$$\mathrm{TDR}(\emptyset) = \tan^{-1}\left(\frac{\partial\emptyset/\partial z}{\sqrt{(\partial\emptyset/\partial x)^2 + (\partial\emptyset/\partial y)^2}}\right)$$

where $\partial\emptyset/\partial x$, $\partial\emptyset/\partial y$, $\partial\emptyset/\partial z$ are the first-order derivatives of the potential field in the $x$, $y$, and $z$ directions, respectively.

The TDR maps of the gravity and the RTP magnetic data of the study area were calculated (Fig. 9). These maps contain high and low closures. It is worth to mention that the zero contour of the TDR map is used to track contacts between causative bodies of lithological variations. The subsurface tectonic framework of the studied area (Fig. 10a) was established based on the integration of all the results. The interpretation of the tilt derivative maps of the gravity and magnetic analyses indicated that the most dominant trends of the area are in the NNW-SSE and E-W directions (Fig. 10b).

## 5. 2D gravity and magnetic forward modeling

The 2D forward modeling of gravity and magnetic data are applied to determine of subsurface geology and the basement relief structure as well as the determination of density and susceptibility of each layer. The geophysical forward modeling of this study was performed based on the methods of Talwani et al. (1959) and Talwani and Heirtzler (1964) which incorporates 2D formulations from Rasmussen and Pedersen (1979). To avoid edge effects, 2D cross sections are extended up to ± 30,000 km along the profile at each extremity of the profile. The density and the magnetic susceptibility values were obtained after the work of Dobrin and Savit (1988), Clark and Emerson (1991) and Hunt et al. (1995). Six long profiles have been selected to cover the study area and were performed using GM-SYS program (2007), a toolkit within Geosoft Oasis Montaj program. The interpreted 2D models are considered from the gravity and the magnetic responses for the same subsurface geological model.

The selected profiles were chosen carefully to cover most of the area and pass through the two drilled boreholes (Table 1 and Fig. 7) in the study area. The final models of the profiles are shown in Fig. 11. A detailed description of the 2D forward modeling sections of the selected profiles is summarized in Table 2.

The six profiles show that the estimated density of the sedimentary cover ranges from 2.31 g/cm$^3$ at D-D′ section to 2.88 g/cm$^3$ at section B-B′, while the estimated magnetic susceptibility ranges from 0.009 SI at the C-C′ section to 0.052 SI at section D-D′. The density of the basement rock ranges from 2.385 g/cm$^3$ at section F-F′ to 2.86 g/cm$^3$ at B-B′ section, while the magnetic susceptibility ranges from 0.01 SI at section C-C′ to 0.049 SI at section D-D′. The sedimentary cover in the study area based on the results of the 2D forward modeling varies from 450 m to 3950 m.

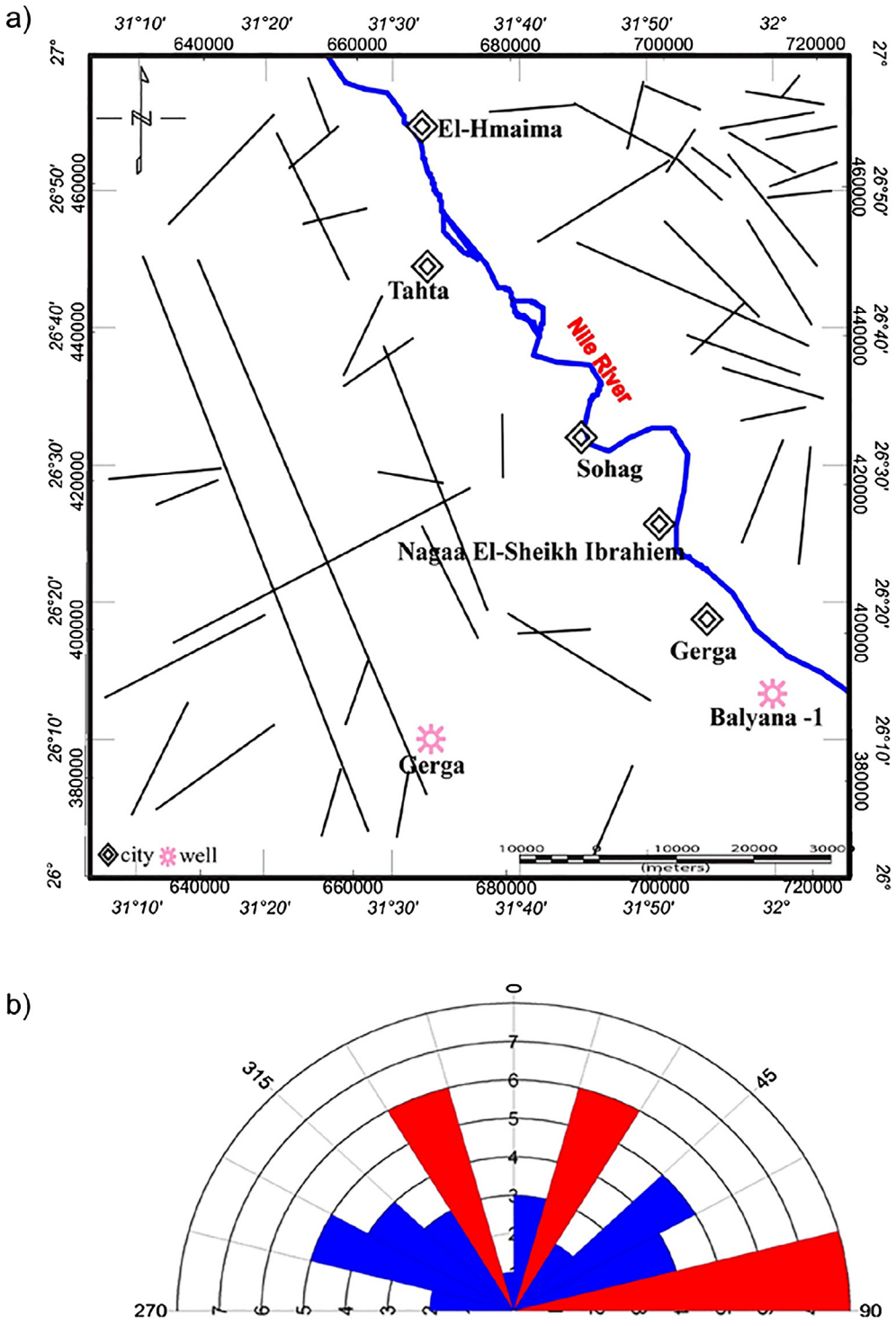


**Fig. 5.** (a) The surface fault structural map extracted from the shaded relief map. (b) Rose diagram shows the main surface structural fault trends in the study area.

The lithological variation denoted by block L1 caused some deviations in gravity and magnetic data interpretation. All modeled sectors reveal that block L1 has density values ranging from 2.396 to 2.876g/cm$^3$ and magnetic susceptibility values ranging from 0.01 to 0.049 SI. Depending on these results and according to Clark and Emerson (1991) and Hunt et al. (1995), these intrusive bodies can be considered as granodiorite rocks.

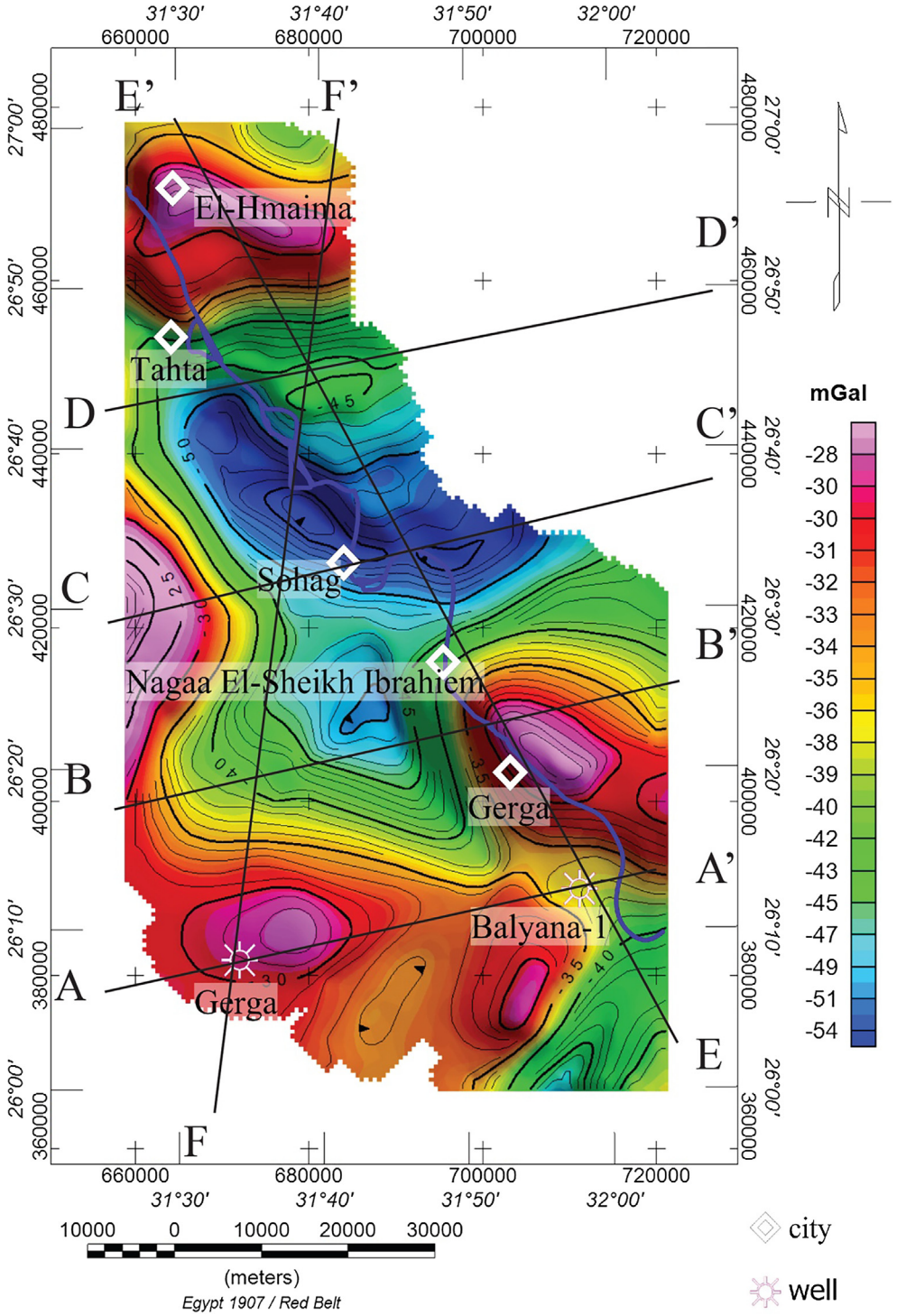


**Fig. 6.** Bouguer gravity map of the study area. Black lines represent locations of the selected profiles for 2D forward modeling.

## 6. Results and discussion

Prior to the present study, there were several attempts by many researchers and authors to investigate the study area (e.g. El-Gamilli, 1964; Mahmoud and Abu-Deif, 1997). The present study is an attempt to give a better understanding of the structural situation of the study area by exploring the surface and subsurface structural elements and their depths.

GIS technique was used as a powerful tool in identifying surface geological structures including fault segments, surface lineaments and their effects on the drainage systems prevailing in the study area. The surface faults, lineaments and drainages were traced out and

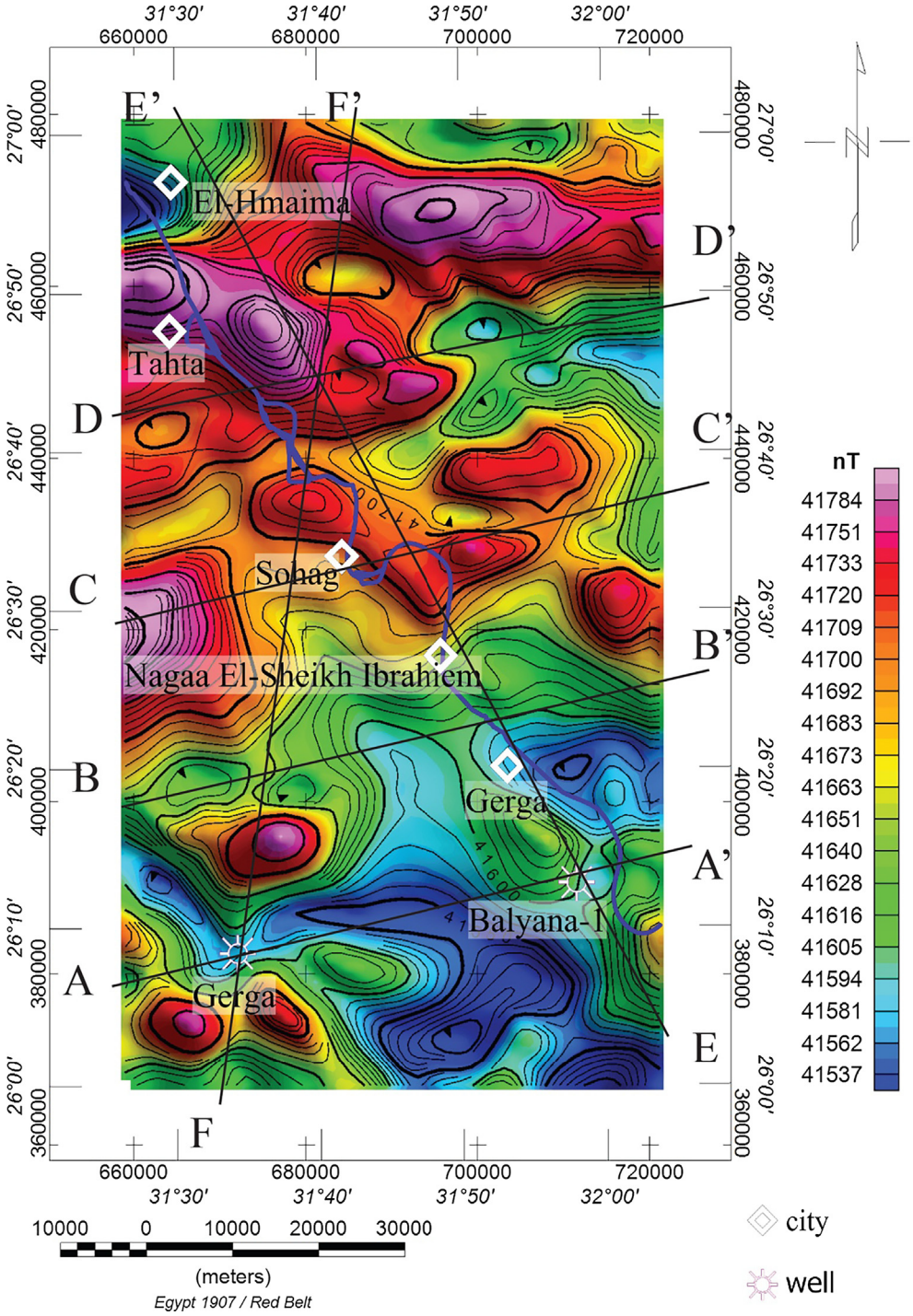


**Fig. 7.** The total magnetic intensity map of the study area. Black lines represent locations of the selected profiles for 2D forward modeling.

statistically analysed to detect the main surface trends affecting the area in decreasing order (Fig. 5b). It is worthy to mention here that most of the traced drainages of long extension are structurally controlled.

The subsurface faults and lineaments were detected through the analysis of the tilt derivative maps of Bouguer gravity and RTP magnetic anomaly data. The tilt derivative maps are powerful techniques that help effectively for detecting dimensions and extensions of the source bodies causing gravity and magnetic anomalies. Hence, the subsurface trends were traced out and also statistically analyzed to represent the interpreted subsurface trends (Fig. 10a and 10b). It shows that interpretation of the subsurface tectonic map of the area indicated the presence of two sets of faults NNW–SSE and E–W which are

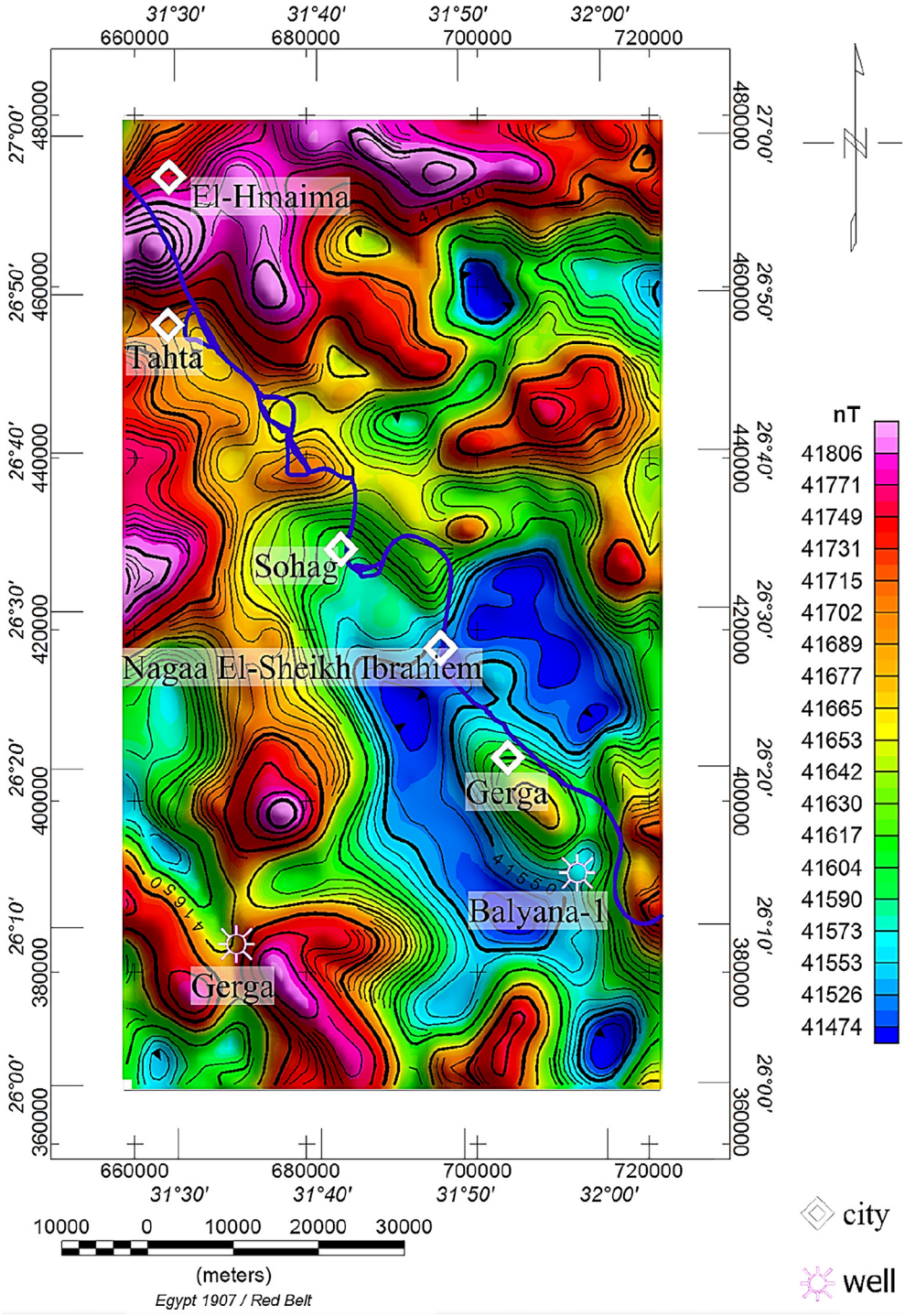


**Fig. 8.** The RTP magnetic map of the study area.

dissected by a NNE–SSW, WNW-ESE and NE-SW fault systems. These two sets of fault systems correspond well with that obtained from the surface structural faults inferred from the GIS model. These results show that there are some faults extend from subsurface to the surface and there is also a principal trend oriented NNW-SSE.

The 2D joint gravity and magnetic forward modeling was carried out along six profiles to cover mostly the entire study area. The 2D modeling technique helps to understand the irregular pattern of the basement of varying depths reflecting uplifted basement (horsts) reaching up to 400 m and down-faulted basins/sub-basins (grabens) reaching up to 4000 m. In general, the basement depth ranges from 400 to 4000 m below ground surface.

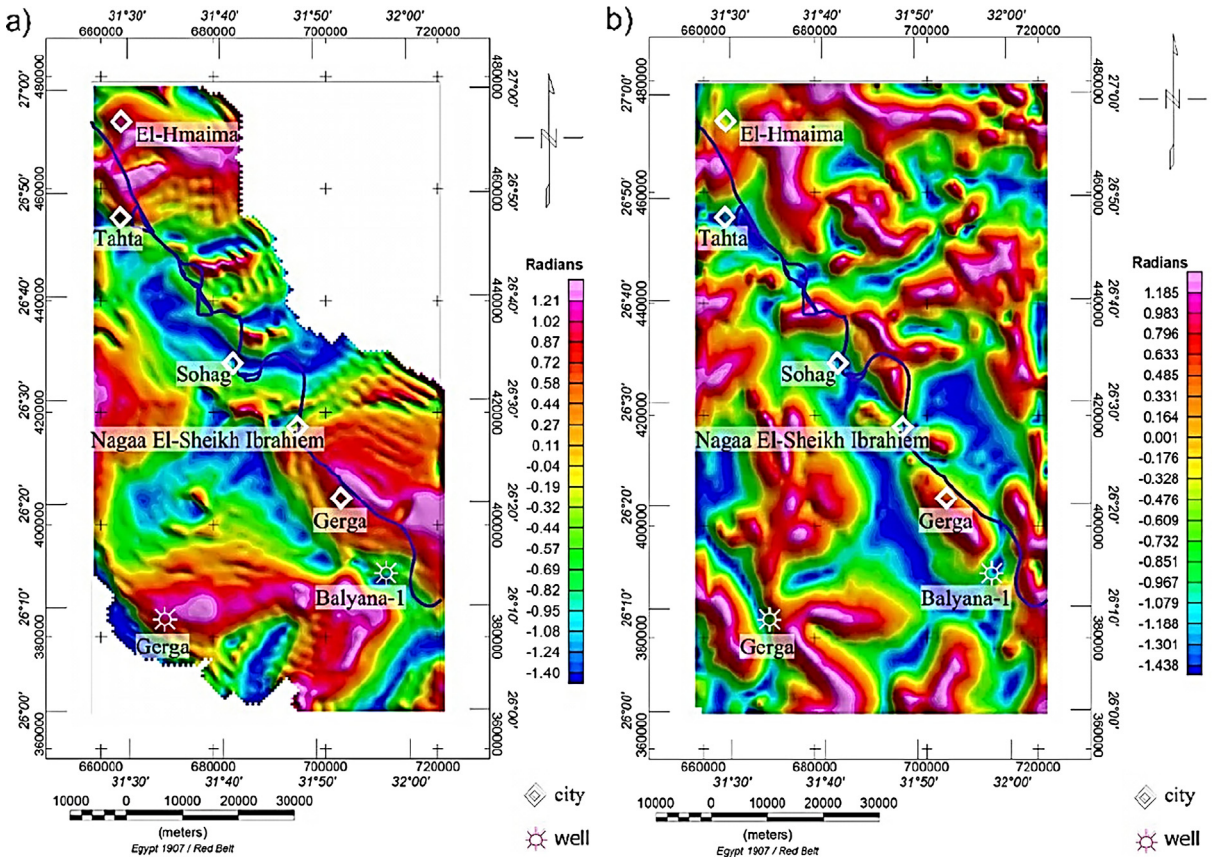


**Fig. 9.** Tilt derivatives of (a) gravity and (b) RTP magnetic maps.

## 7. Conclusion

In this study, several geophysical methods were used to investigate surface and subsurface structural conditions in the study area. The structure fault segments maps, that were extracted from the GIS model and the tilt derivative technique, show that there is a good correlation and distribution of the fault segments and faults lines (previously known fault lines) and also, present that the study area is affected by several main faults trending E-W, NNW-SSE, and NNE-SSW where NNW-SSE is the major trend in the study area. The depth to the surface of the basement in the area ranges from 400 to 4000 m where the average depth value at Sohag basin is 3500 m. Some intrusive bodies were recorded along the modeling profiles indicating to granodiorite rock type.

## Acknowledgements

The authors would like to thank the Editor and two anonymous reviewers for their constructive comments that have greatly improved the manuscript. The second author (Dr. Ibraheem) is hugely indebted to the International Institute of Education-USA and the University of Cologne - Germany for hosting him as a postdoctoral academic visitor.

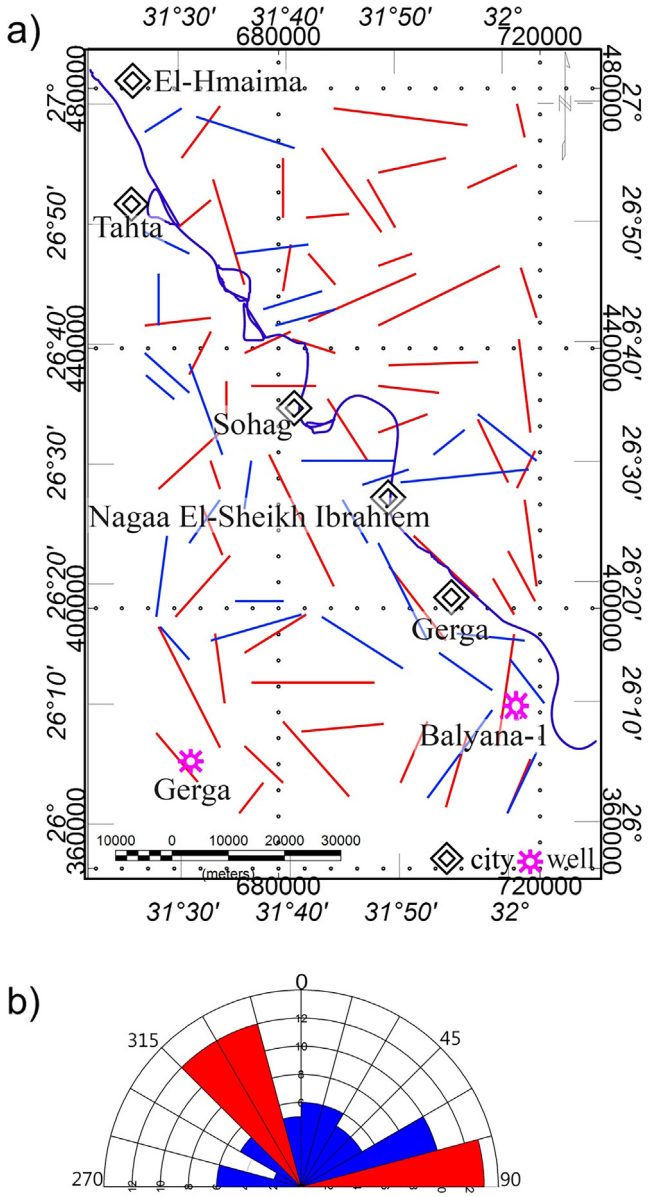


**Fig. 10.** (a) Structural map extracted from the tilt derivatives of gravity (blue lines) and RTP magnetic (red lines) maps. (b) Rose diagram shows the fault trends in the study area. (For interpretation of the references to colour in this figure legend, the reader is referred to the web version of this article.)

**Table 1**
Data of the exploratory wells in the study area (Nabih, 1997).

| Well name | Latitude | Longitude | Rock unit | T.D (m) | Depth to basement (m) |
|---|---|---|---|---|---|
| Balyana-1 | 26°13′24.7″ | 31°58′32.2″ | Basement | 1737 | 1640 |
| Gerga | 26°09′00″ | 31°30′00″ | Eocene | 492 | – |

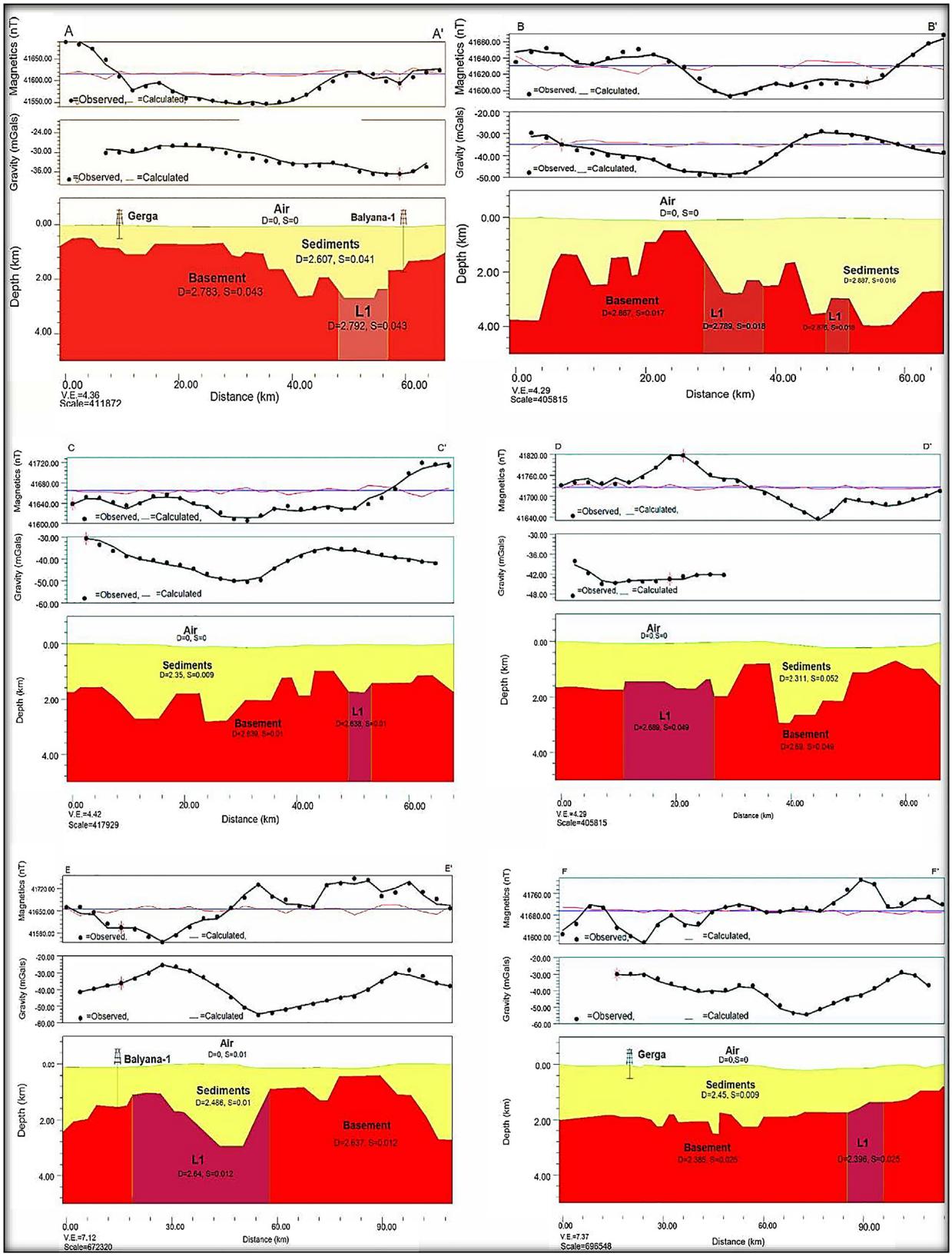


**Fig. 11.** 2D Gravity and magnetic models for profiles AA′, BB′, CC′, DD′, EE′ and FF′.

**Table 2**
Description of 2D gravity and magnetic modeling sections.

| Profile | Length (km) | Density range (g/cm$^3$) | | Susceptibility range (SI) | | Depth to basement (m) |
|---|---|---|---|---|---|---|
| | | Sediments | Basement | Sediments | Basement | |
| A-A′ | 67.7 | 2.607 | 2.762–2.792 | 0.041 | 0.043 | 800–2680 |
| B-B′ | 68.66 | 2.887 | 2.789–2.867 | 0.016 | 0.017–0.018 | 450–3950 |
| C-C′ | 68.74 | 2.35 | 2.638–2.639 | 0.009 | 0.01 | 970–2800 |
| D-D′ | 67.81 | 2.311 | 2.69–2.689 | 0.052 | 0.049 | 770–2950 |
| E-E′ | 109.75 | 2.486 | 2.637–2.64 | 0.01 | 0.012 | 380–2970 |
| F-F′ | 113.74 | 2.45 | 2.385–2.396 | 0.009 | 0.025 | 470–2520 |

## References


Abdullah, A., Nassr, S., Ghaleeb, A., 2013. Remote sensing and geographic information system for fault segments mapping a study from Taiz Area, Yemen. J. Geol. Res. http://dx.doi.org/10.1155/2013/201757.

Aero Service Division of the Western Geophysical Company of America, 1983. The total magnetic intensity map of Egypt. Scale of 1: 50,000.

Clark, D.A., Emerson, D.W., 1991. Notes on rock magnetization characteristics in applied geophysical studies. Explor. Geophys. 22, 547–555.

Conoco, 1987. Geologic map of Egypt NG 36 NW Asyut (Scale 1: 500000). General Petroleum Company, Cairo, Egypt.

Dobrin, M.B., Savit, C.H., 1988. Introduction to Geophysical Prospecting, 4th ed. McGraw-Hill Book Co., New York.

El-Gamilli, M., 1964. Geological and geophysical studies on wadi El-Assuity area, Eastern Desert, Egypt. MSc. Thesis, Assuit University, Egypt.

EL-Sherief, M.A.M.M., 2016. GIS-based 3D source/reservoir rocks evaluation of selected Mesozoic Formation, North Western Desert (Egypt) integrating well logs and geo-chemical data. M.Sc. thesis, department of Geology, Faculty of Science, Tanta University, Tanta, Egypt, pp. 135–226.

General Petroleum Company, 1977. Bouguer gravity map of Egypt; scale 1:100,000.

Hunt, C.P., Moskowitz, B.M., Banerjee, S.K., 1995. Magnetic properties of rocks and minerals. In: Rock Physics and Phase Relations - A handbook of Physical constants. AGU Reference shelf 3.

Ibraheem, I.M., 2005. Structural studies on the northern part of Sinai using the potential field methods. M.Sc. thesis, Ain Shams University, Cairo, Egypt.

Ibraheem, I.M., 2009. Geophysical potential field studies for developmental purposes at El-Nubariya – Wadi El-Natrun, West Nile Delta, Egypt. Ph.D thesis, Faculty of Science, Mansoura University, Mansoura, Egypt.

Ibraheem, I.M., Elawadi, E.A., El-Qady, G.M., 2018a. Structural interpretation of aero-magnetic data for the Wadi El Natrun area, northwestern desert, Egypt. J. Afr. Earth Sci. 139, 14–25. http://dx.doi.org/10.1016/j.jafrearsci.2017.11.036.

Ibraheem, I.M., Gurk, M., Tougiannidis, N., Tezkan, B., 2018b. Subsurface investigation of the neogene mygdonian basin, Greece using magnetic data. Pure Appl. Geophys. http://dx.doi.org/10.1007/s00024-018-1809-x.

Mahmoud, F.A., Abu-Deif, A.M., 1997. Subsurface geologic conditions in the area south west of Sohag for petroleum potentialities. In: The 2nd international scientific conference on science, environment and sustainable development, Faculty of Science, Al Azhar University, Cairo, Egypt.

Mao, Y., Ye, A., Xu, J., Ma, F., Deng, X., Miao, C., Gong, W., Di, Z., 2014. An advanced distributed automated extraction of drainage network model on high-resolution DEM. J. Hydrol. Earth Syst. Sci. Discuss. 11 (7), 7441–7467. http://dx.doi.org/10.5194/hessd-11-7441-2014.

Miller, H.G., Singh, V., 1994. Potential field tilt – a new concept for location of potential field sources. J. Appl. Geophys. 32, 213–217.

Nabih, N., 1997. Exploratory Well Data of Egypt, Cairo, Egypt, pp. 4–38.

Oruç, B., Keskinsezer, A., 2008. Structural setting of the northeastern Biga Peninsula (Turkey) from tilt derivatives of gravity gradient tensors and magnitude of horizontal gravity components. J. Pure Appl. Geophys. 165 (9–10), 1913–1927.

Rasmussen, R., Pedersen, L.B., 1979. End corrections in potential field modeling. Geophys. Prospect. 27 (4), 749–760.

Said, R., 1962. The geology of Egypt. Elsevier, Amsterdam, p. 377.

Said, R., Wendorf, F., Schild, R., 1970. The geology and prehistory of the Nile Valley in Upper Egypt. Archaeol. Polona. 12, 43–60.

Shahverdi, M., Namaki, L., Montahaei, M., Mesbahi, F., Basavand, M., 2017. Interpretation of magnetic data based on Tilt derivative methods and enhancement of total horizontal gradient, a case study: Zanjan Depression. J. Earth Space Phys. 43 (1), 101–113.

Talwani, M., Heirtzler, J.R., 1964. Computation of magnetic anomalies caused by two-dimensional structures of arbitrary shape. In: Computers in the mineral industries. Part 1: Stanford University Publications, Geological Sciences, 9, 464–480.

Talwani, M., Sutton, G.H., Worzel, J.L., 1959. A crustal section across the Puerto Rico trench. J. Geophys. Res. 64 (10), 1545–1555.

Telford, W.M., Geldart, L.P., Sheriff, R.E., 1990. Applied Geophysics, 2nd ed. Cambridge University Press, pp. 26–117.

Wendorf, F., Schild, R., 1976. The use of ground grain during the Late Paleolithic of the Lower Nile Valley, Egypt. In: Harlan, J.R. (Ed.), Origins of African Plant Domestication, De Gruyter Mouton, pp. 269–288.

Yehia, M.A., Hassan, O.A., Hamdan, A.H., Ashmawy, M.H., Hermas, E.A., El-Etr, H.A., 1999. Geo-Environmental study of the Sohag-Lake Nasser stretch, Egypt. Egypt. J. Rem. Sens. Space Sci. 2, 1–14.

Youssef, M.I., 1968. Structural pattern of Egypt and its interpretation. Am. Assoc. Petrol. Geol. (AAPG) Bull. 52 (4), 601–614.